DOI 10.5162/ettc2022/8.1

Evaluation of Solar-based Energy Harvesting for Indoor IoT Applications

Leander B. Hörmann[1], Thomas Hölzl[1], Christian Kastl[1], Peter Priller[2], Hans-Peter Bernhard[3], Philipp Peterseil[4], Andreas Springer[4]
[1] Linz Center of Mechatronics GmbH, Altenberger Straße 69, 4040 Linz, Austria,
[2] AVL List GmbH, 8020 Graz, Hans-List-Platz 1, Austria,
[3] Silicon Austria Labs GmbH, Altenberger Straße 69, 4040 Linz, Austria,
[4] Institute for Communications Engineering and RF-Systems, Johannes Kepler University Linz, Altenberger Straße 69, Austria, 4040 Linz
Leander.Hoermann@lcm.at

Abstract:
Internet-of-Things (IoT) devices and other embedded devices are more and more used to measure different conditions inside of buildings and industrial facilities as well as to monitoring machines or industrial processes. IoT sensors communicate wirelessly and are typically supplied by batteries. Energy harvesting can be used to extend their operational time or enable self-sufficient supply of them. Energy from the environment is converted into electrical energy by energy harvesting devices (EHDs), for example solar cells or thermo-generators. However, the available output power of the EHDs is highly dependent on the mounting location as well as on environmental conditions and may vary greatly over time. Therefore, it is meaningful to evaluate the EHDs at the location of use over a certain period of time in order to characterize them in real world scenarios. This paper presents the evaluation setup and the results of the characterization of four different solar cells at different locations in an office building and at different weather conditions. Furthermore, a method is presented to estimate the possibility to supply embedded device using energy harvesting. The results can be used to simplify the selection of a suitable EHD and the design process of an energy management system. The method is applied on two different use cases to estimate the needed size of the solar cells to enable a continuous supply.

Key words: Internet-of-Things, wireless communication, energy harvesting, self-sufficient.

Introduction

In the last years, Internet-of-Things (IoT) spreads rapidly and reached more and more new application areas. The advances in ultra-low power electronics and wireless communication are key enabling technologies for this development. The IoT connects wireless embedded devices to the internet. Such devices could be sensors or actuators and application areas reach from smart buildings and home automation over smart farming to industrial application where they are often referred as industrial IoT (IIoT). Especially, sensors are predestinated to be implemented as IoT or IIoT devices since a lot of them could be used to monitor the surrounding inside a smart building or industrial machines and processes. They are than often called “sensor nodes”, measure physical quantities, and transmit them wirelessly towards a gateway using a certain communication protocol [1], [2]. These sensor nodes should be powered without a wired connection to reduce cost, enhance the flexibility and handling, enable an easy encapsulation for e.g., water tightness, and to reach application areas where cabling is not possible. Thus, they can be powered in two different ways, by batteries and by energy harvesting [3]. Using batteries, the needed energy is supplied with the installation of the sensor nodes and operational time is limited but guaranteed. In this paper, we focus on the second possibility. Using energy harvesting devices (EHDs), the needed power to supply the sensor nodes is converted from power available in the environment, e.g., solar or artificial light or temperature gradients. By using energy harvesting, the theoretical operational time of the embedded devices is not limited. However, the harvestable electrical power of the environment is highly variable [4], [5]. Therefore, an energy storage is needed to provide a continuous supply of the wireless sensor node, e.g., rechargeable batteries or supercapacitors. If the capacity is well dimensioned, a perpetual operation is achievable [6].

Illumination-based environmental power sources are typically available in office buildings and factories since they are regularly used by humans. Natural sunlight is available on a daily base but

varies with weather and season. Artificial light is available only during the regular working time which is often on a weekly base. Furthermore, the convertible power depends also on the location inside a building. To characterize the convertible power of EHDs directly on location over a certain period of time, we have developed a characterization instrument which we have presented in [7] and evaluated in [8]. This paper presents the results of measurement campaign for indoor scenarios focusing on solar-based energy harvesting at different locations. These results can be used to estimate the available energy for different application scenarios.

The rest of the paper is organized as follows: First, this paper gives an overview of the measurement system, second, it describes the measurement campaign including the location dependent and the time dependent evaluation, and third, it discusses the applicability of the measurement results on two different use cases. Finally, it concludes the paper and outlines directions for future work.

Measurement System for the Characterization of Energy Harvesting Devices

The measurement system is designed to characterize EHDs automatically and autonomously. Thus, it can be used to characterize EHDs directly on site. The characterization is based on a cyclic acquisition of the current-voltage characteristics of the connected EHDs. The measurement interval and the number of measurement points to be recorded can be configured. The characterization results are transmitted wirelessly towards a base station using a mesh network. The autonomous measurement device is shown in Fig. 1.

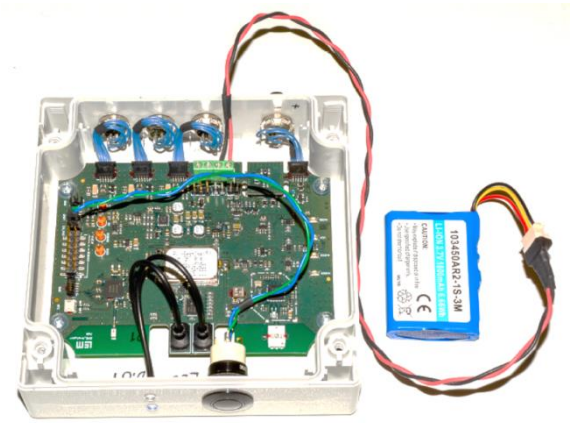

Fig. 1: Autonomous characterization instrument for energy harvesting devices.

The main parts of the measurement device are the nRF52840 system-on-chip containing a microcontroller and a transceiver circuitry for wireless communication, a power supply circuitry including the Lithium-Ion rechargeable battery, and the measurement circuitry. The measurement circuitry characterizes the EHDs using a variable load for setting different operating points. The voltage for each operating point is set by the microcontroller and a digital-to-analog converter. The resulting voltages and currents at the EHD are measured using an analog-to-digital converter. The supported voltage ranges from below 1 mV up to 24 V in two measurement ranges. The supported current ranges from below 1 µA up to 1 A in three measurement ranges which are automatically selected using an analog comparator circuit. A detailed analysis of the mode of operation and achieved accuracies is given in [8].

Measurement Campaign

The measurement campaign was performed inside an office building in Linz, Austria with the coordinates N 48.335902 and E 14.322516. The campaign consists of different short-term measurements at different location in two different rooms (one south aligned, and one north aligned) and on different days in the summer (between 22nd and 26th of July 2021) with different weather conditions (sunny and foggy days). A rough ground floor plan of the relevant part of the office building including the two rooms are shown in Fig. 2.

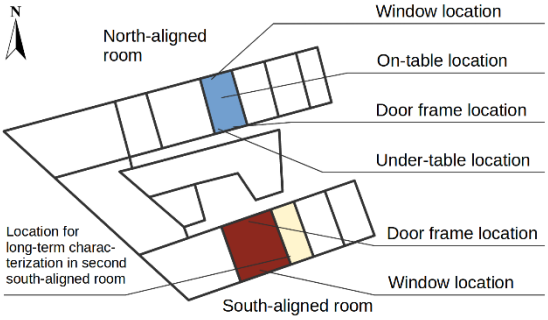

Fig. 2: Floor plan of the relevant part of the building showing the orientation of the rooms and indicating the locations of the measurements.

At all locations, four different solar cells have been evaluated: YH-46x76 from Conrad components with an active area of 11.78 cm² [9], YH-57x65 from Conrad components with an active area of 30.87 cm² [10], SM141K10LV from IXYS with an active area of 16.2 cm² [11], and SM141K09L from IXYS with an active area of 14.49 cm² [12]. Due to insufficient output power at locations with bad illumination conditions, not all solar cells could be characterized at all locations and at all weather conditions. The results are shown in the following section.

Location Dependent Evaluation

The location dependent evaluation was performed at two different locations at the south aligned room and at four different locations at the north aligned room. Fig. 3 shows the power density of the solar cells placed directly on the window facing outwards at the south aligned room.

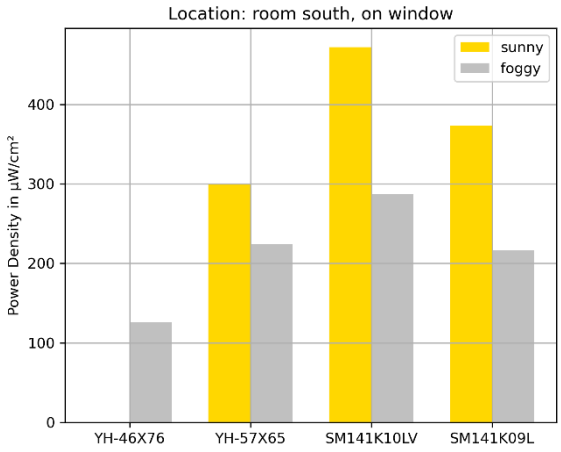

Fig. 3: Power density of the solar cells placed on the window at the south aligned room.

Fig. 4 shows the power density of the solar cells placed on the doorframe on the opposite side of the windows facing to the windows at the south aligned room.

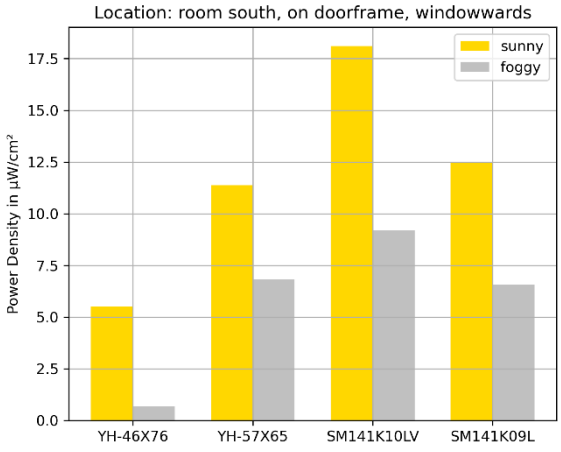

Fig. 4: Power density of the solar cells placed on the doorframe at the south aligned room.

Fig. 5 shows the power density of the solar cells placed directly on the window facing out-wards at the north aligned room.

Fig. 6 shows the power density of the solar cells placed on the doorframe on the opposite side of the windows facing to the windows at the north aligned room.

Fig. 7 shows the power density of the solar cells placed on a table in the middle of the north aligned room facing upwards.

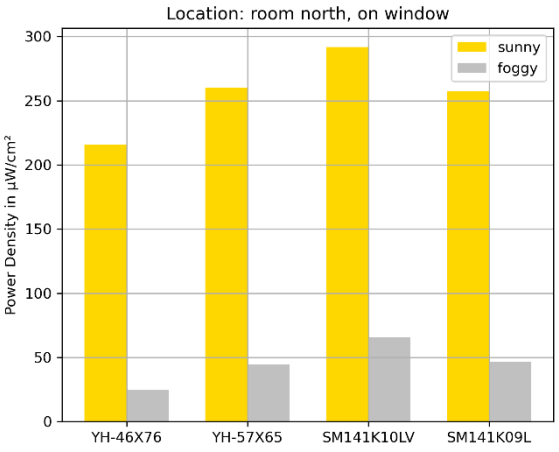

Fig. 5: Power density of the solar cells placed on the window at the north aligned room.

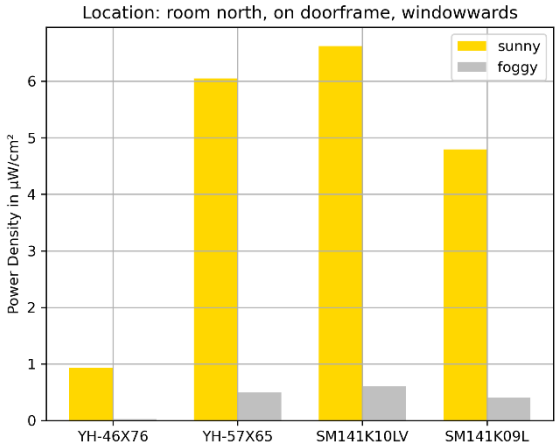

Fig. 6: Power density of the solar cells placed on the doorframe at the north aligned room.

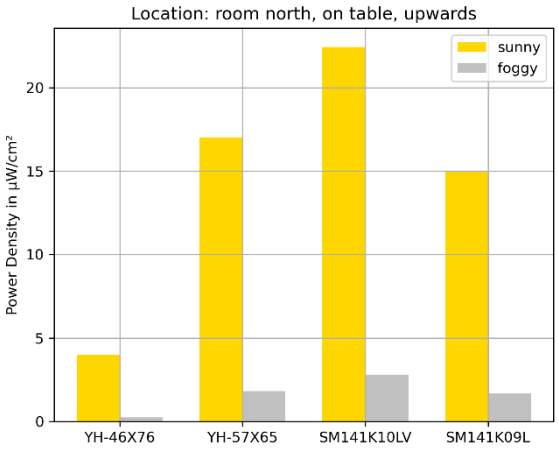

Fig. 7: Power density of the solar cells placed on a table in the middle of the north aligned room.

Fig. 8 shows the power density of the solar cells placed on the floor under a table on the opposite side of the windows of the north aligned room facing upwards. A measurement at foggy conditions was not possible due to insufficient power output of the solar cells.

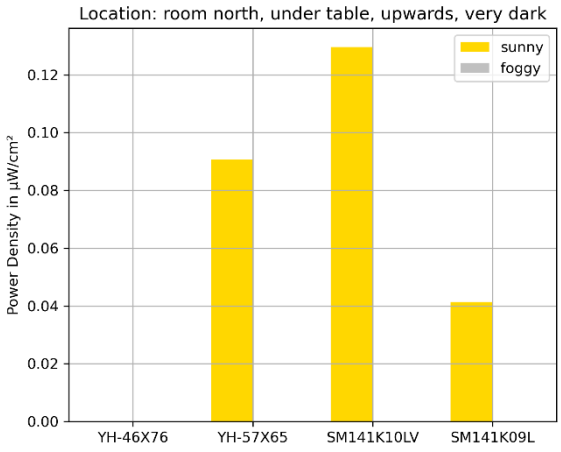

Fig. 8: Power density of the solar cells placed under a table in the north aligned room.

The results are summarized for the best performing solar cell (SM141K10LV) and compared in Tab. 1. The given percentage refers to the maximum achievable power (obviously at the window) for each room. It depends mainly on the geometry, the window placement, and the interior of the room. There is a big difference between the best placement for energy harvesting at the window and the opposite side of the room with a factor of 26.1 to 44.1. At very dark locations (e.g., in a dark corner under the table), the power density is again significantly reduced by a factor of 50.9 compared to the location at the doorframe resulting in a total factor of 2245 compared to the optimal window location. This factor can be seen as a location dependent inter-room factor.

Tab. 1: Power density of the best performing solar cell SM141K10LV at different locations.

Location	Power density in µW/cm²	Percentage referring to maximum in room
South, window	472.04	100 %
South, doorframe	18.11	3.84 %
North, window	291.85	100 %
North, doorframe	6.62	2.27 %
North, on table	22.44	7.69 %
North, under table	0.13	0.045 %

Time Dependent Evaluation

The time dependent evaluation focuses on the determination of the daily change of harvestable power and total harvestable energy over a day. Therefore, the solar cell AM-1815CA from Sanyo with an active area of 26.22 cm² [13] is placed at the wall beside the window (on the side wall of the room) of the south aligned room. Fig. 9 shows the harvestable power of the solar cell during a sunny day (13th of April 2022, 12.2 hours of sun). During this day, the harvestable energy sums up to 45.24 J which corresponds to an average harvestable power of 523.6 µW or 19.97 µW/cm².

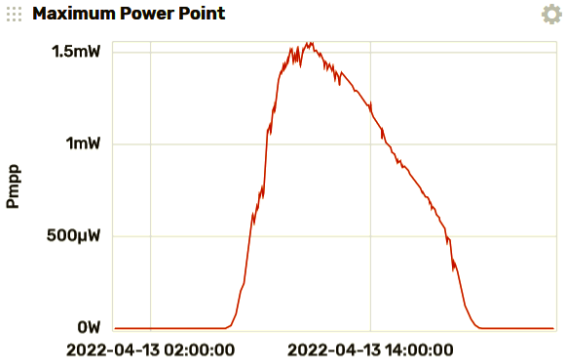

Fig. 9: Harvestable power of the solar cell AM-1815CA over a sunny day.

Fig. 10 shows the harvestable power of the same solar cell during a day without sun (22nd of April 2022, 0 hours of sun). During this day, the harvestable energy sums up to 18.75 J which corresponds to an average harvestable power of 278.25 µW or 10.61 µW/cm². This results in a weather dependent factor of 41.4 % compared to sunny weather conditions. However, the measurement period must be extended to a whole year and a detailed analysis regarding the seasonal weather variations has to be done.

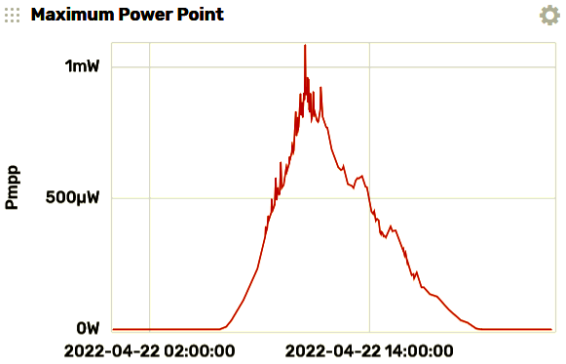

Fig. 10: Harvestable power of the solar cell AM-1815CA over day without sun.

Fig. 11 shows the harvestable power of the solar cell during a 13-day period with different weather conditions (from 12th to 24th of April 2022). During this period, the harvestable energy sums up to 422.18 J which corresponds to an average harvestable power of 375.9 µW or 14.34 µW/cm². It can be seen that the weather dependent variation is orders of magnitude

smaller than the location dependent variation inside a room. From previous measurements with a different measurement hardware presented in [3] the seasonal dependent factor ranges approximately from 16.7% to 26.7% between sunny weather condition in summer and winter.

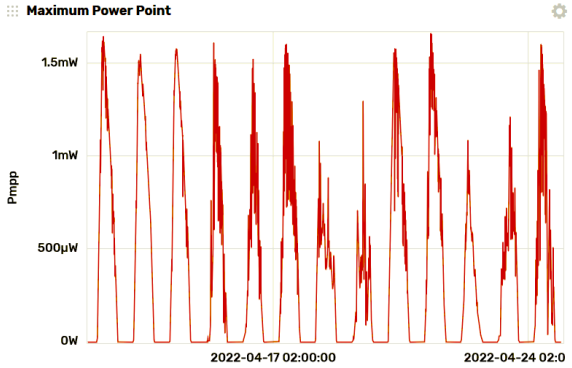

Fig. 11: Harvestable power of the solar cell AM-1815CA during a 13-day period (from 12th to 24th of April 2022).

Supply Possibility Analysis by Means of Energy Harvesting

To analyze the possibility to supply an embedded device using energy harvesting, the following information must be known as also presented in [14]: the trace of the harvestable power P_{EH}, the trace of the consumed power of the embedded device P_{SUP}, the capacity of the energy storage device in terms of energy $E_{BAT,max}$, and the amount of energy stored in the energy storage device $E_{BAT,0}$ at time step $n=0$. Starting from time step $n=1$, the energy stored in the energy storage device for the next time step $E_{BAT,n}$ is calculated. For this purpose, the stored energy of the last time step $E_{BAT,n-1}$, the measured input power in this time step $P_{EH,n}$ and the expected output power in this time step $P_{SUP,n}$ are taken into account as shown in (1).

$$E_n = E_{BAT,n-1} + \left(P_{EH,n} \cdot \eta - P_{SUP,n}\right) \cdot \Delta t \quad (1)$$

The factor η describes the efficiency of the energy harvesting circuit since losses occur during the DC-DC conversion and storage of the electrical energy. Furthermore, the calculated energy must be limited to the maximum capacity of the energy storage $E_{BAT,max}$ as shown in (2).

$$E_{BAT,n} = \min\left[E_{BAT,max}\ ,\ E_n\right] \quad (2)$$

For each time step $n > 0$ this energy must be greater than 0 as shown in (3).

$$E_{BAT,n} > 0 \quad for\ n = 1,2,\ldots \quad (3)$$

Not considered here is the self-discharge of the energy storage device. The energy stored in the energy storage device is calculated iteratively for each time step n. If the calculated energy is greater than 0, then continuous operation till this time step n is possible.

Based on equation (1), it can be seen that if the second term is greater zero, the energy stored in the energy storage device will never run out of energy and a perpetual operation is possible. Simplifying this by using the average harvestable power $P_{EH,avg}$ and the average consumed power $P_{SUP,avg}$, and considering enough energy storage capacity, it can be reduced to the equation shown in (4).

$$P_{EH,avg} \cdot \eta > P_{SUP,avg} \quad (4)$$

Use Case Automotive Testing

Academic and industrial research have demonstrated the benefits of using IoT in industrial applications [15] [16]. Use cases in mobility, industrial, and smart city domains, for example, clearly benefit from wireless connectivity, which allows dynamic placement, saves cost and weight of cables, and often allows even tighter integration into components.

Automotive test factories provide good examples for a particularly worthwhile, but also challenging use case, and have been studied in more detail in [2]. Such facilities are widely used across the automotive industry for research, development and quality control accompanying production. Test factories for batteries in electrical vehicles, for example, are used to explore the relevant properties of battery cells, modules, or racks, in order to improve and validate their design. Powertrain test beds allow to analyze engines (E-Motor or ICE) and transmissions to study and improve efficiency, performance, vibration (comfort), degradation patterns, and aging. Other examples include full vehicle testbeds to develop advanced driving assistance systems (ADAS) and automated driving functionalities (AD), or component test beds used for example to optimize the thermal system in a vehicle.

These use cases typically deploy a wide range of sensors, which need to be placed on, or even integrated into the systems under test (SUT). Using wireless sensor networks (WSNs) to instrument SUTs has demonstrated clear cost advantages due to a significant reduction of the time required for installation and configuration. In addition, typical sources of failures, like poor connectors or miswiring issues, are eliminated, further contributing to improved productivity in test fields operations.

A critical part however is adequate energy supply of the nodes. The desired operational time of

an IoT node might vary from hours to weeks. Some test sequences allow the node to power down between phases. Others require continuous 24x7 operation, resulting for example in 720 hours runtime per month. Some current solutions rely on batteries to power nodes locally; in combination with highly energy-efficient communication protocols and ultra-low power hardware design, batteries provide sufficient operating time for a subset of scenarios. Energy supply must be ensured for the full time an SUT is deployed in the test scenario, as power failure would likely lead to a loss of experimental data, rendering the whole test worthless. A change of batteries is often impossible due to operational needs. The promise of continuous energy supply for nodes using EHDs is therefore highly welcome. Many test cells are typically well-lit laboratory environments, with levels of luminous intensity comparable with or even exceeding typical indoor office conditions.

However, it is necessary that the IoT nodes are based on ultra-low power electronics and are wirelessly connected using an energy efficient communication protocol. In [2] we have introduced an Energy and Power Efficient SynchrOnous wireless Sensor network (EPHESOS) protocol. This protocol is especially designed for wireless sensor networks requiring on average low power and at the same time defined latency. Low power consumption is achieved by using a time division multiple access (TDMA) protocol which enables tightly synchronized wireless sensor nodes. Thus, the transmission and reception times with powered transceiver circuitry of each individual sensor nodes can be minimized. The TDMA structure is based on a frame called superframe (SF) with pre-allocated time slots for each sensor node to transmit sensor data and one time slot used by the base station addressed as wireless network processor (WNP) to transmit a beacon to all sensor nodes. This beacon time slot is one timeslot per SF in which the sensor nodes are receiving data synchronously. The individual sensor node time slots are used for transmitting sensor data. The nodes remain in sleep mode whenever they are not receiving or transmitting. The communication protocol supports two different modes, which are briefly explained below: First, the sporadic transmission mode, EPhESOS-S, is responsible for network commissioning, integration of new nodes, initial synchronization, node configuration and maintenance. Second, the continuous transmission mode, EPhESOS-C, is used to transmit measurement data from the nodes towards the WNP in their own time slots. If a packet is lost, the incorrectly received or missing value is added to the next packet and sent again in the following SF.

We have designed and implemented wireless sensor nodes based on an nRF52840 system-on-chip (SoC) which integrates a processing unit and a wireless transceiver for 2.4 GHz radio frequency (RF) communication. It uses the EPhESOS communication protocol for wireless communication. Furthermore, the sensor node contains an analogue-to-digital converter with an associated analogue circuit. The analogue circuitry is designed to support Pt100, Pt1000 and thermocouple temperature sensors as described in [17]. Fig. 12 shows the average power consumption of the wireless sensor node at different measurement modes and temperatures.

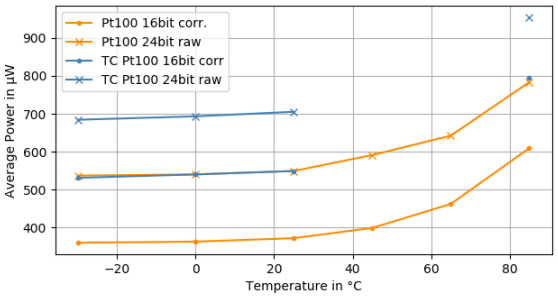

Fig. 12: Average power consumption of the wireless sensor node at different measurements modes and different temperatures.

For a further estimation of the ability to supply the wireless sensor node using energy harvesting, we will use the average power consumption of the measurement mode “Pt100 24bit raw” at 25°C which is 549 µW. In this mode, a Pt100 sensor is sampled with 10 Hz and the results are transmitted with 1 Hz. Considering further a supply a table conditions in a south-aligned room. The average harvestable power can be estimated by multiplying the optimal harvestable power density in this room ($S_{EH,opt}$ = 472.04 µW/cm²) with the location dependent factor (f_{Loc} = 0.0769) and the weather dependent factor ($f_{Weather}$ = 0.414) as shown in (5). Since the measured harvestable power is given per square centimeter, it is a power density and the symbol *S* will be used instead of the symbol *P*.

$$S_{EH} = S_{EH,opt} \cdot f_{Loc} \cdot f_{Weather} = 15.03 \frac{\mu W}{cm^2} \quad (5)$$

Considering an energy conversion efficiency of η = 80% and an operation only during daytime, the needed solar cell area is calculated as in (6).

$$A_{Solar} = \frac{P_{SUP,avg}}{S_{EH} \cdot \eta} = 45.7 cm^2 \quad (6)$$

The resulting area is not that small but can be reduced by reducing the sample frequency or enhancing the illumination conditions. However, this result shows, that under reasonable conditions the power supply of a wireless sensor node can solely rely on energy harvesting based on solar cells.

Use Case User Tracking and Access Authentication

Localization and tracking of persons and assets are services with a huge application potential. Localization systems based on radar or LIDAR (Light detection and ranging) demand large amounts of power, are usually costly, but have a high localization precision. If precision in the millimeter-range is not required, low-power and low-cost wireless localization systems, usually based on Time of flight (ToF), are preferred. During the last years, Ultra-Wideband (UWB) devices have been adopted in many localization systems due to their relatively high ranging precision and low cost. The high bandwidth of UWB enables time of flight measurements with high resolution [18] and thus makes high precision indoor localization possible. UWB impulse radio (IR) enables the implementation of low complexity and low-power transceivers, which translates into low-cost devices.

For access authentication of users, one wants to combine conventional user authentication by means of a cryptographic method with the location of the user. E.g. a cryptographically authenticated user is only granted access to a restricted area if the user in within a certain area to prevent relaying attacks. UWB IRs can be applied here also, because with their ranging capabilities so-called distance bounding (DB) protocols can be executed. DB protocols are employed such that a verifier node (V) can authenticate a prover node (P) with cryptographic methods and at the same time ensure that P is close enough to V by setting an upper bound to its distance to the verifier [19].

We have developed wireless sensor nodes (Fig. 13) based on the DWM1001C UWB-module (1.) which consists of a Bluetooth Low Energy (BLE) capable Nordic nRF52832 microcontroller, a Qorvo DW1000 UWB transceiver and antennas for both standards.

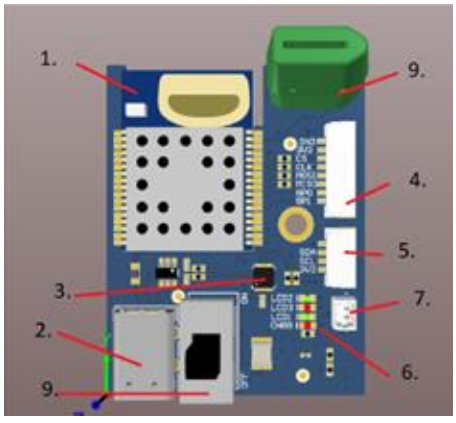

Fig. 13: Wireless sensor node.

Our sensor nodes provide the supply voltage via USB-C (2.) as well as a virtual COM-port (VCP) interface (3.). The extension connectors (4.) and (5.) allow to connect external peripherals via I²C and SPI. With these wireless sensor nodes, UWB-based ranging and DB protocols can be executed and in addition data can be transmitted to base stations or other nodes via BLE. To figure out if a wireless localization and tracking system can be operated solely based on energy harvesting, we performed power measurements. To this end we conducted so-called double-sided two-way ranging (DS-TWR) rounds between two nodes. In an operational localization system, one node would be an anchor, i.e. a node with known position, and the other node would be the tag, which the systems wants to localize by performing ranging with a set of anchors. In a DS-TWR round, the tag transmits a short packet, receives the answer from the anchor, and transmits again. From the two received packets, the anchor estimates the distance and transmits the result back to the tag. In our implementation, such a DS-TWR round has a duration of 11.15 ms and consumes 3.22 mWs of energy at the tag if operated at 3 V. Most energy is consumed during the reception mode of the tag with an average power consumption of approx. 450 mW for 3.5 ms. According to the data sheet of the DWM1001C module [20], the minimum achievable current consumption in the sleep mode is only 12 µA which will be used in further estimation. However, one needs to consider, that both, our design of the node and also the firmware which implements the DS-TWR procedure is currently not optimized for low power. By triggering this procedure using the integrated accelerometer, the average ranging frequency can be reduced and thus, also the power consumption. We will use here the same assumption about the location as at the previous use case and use the power density S_{EH} = 15.03 µW/cm². By assuming a full DS-TWR round every 30 seconds to four anchor nodes, the average power consumption is 465.28 µW. Considering an energy conversion efficiency of η = 80% and an operation only during day, the needed solar cell area is calculated as shown in (7).

$$A_{Solar} = \frac{P_{SUP,avg}}{S_{EH} \cdot \eta} = 38.7 cm^2 \qquad (7)$$

Considering, that neither node hardware nor DS-TWR protocol is optimized for low-power operation, this result clearly shows that under reasonable conditions the power supply of a tag of a UWB-based localization system can solely rely on energy harvesting based on solar cells.

Conclusion

This paper presented the evaluation of four different solar cells as energy harvesting devices in a real-world environment at different locations in two different rooms of an office building. The results can be used to estimate the location-based influence on the harvestable energy. Furthermore, an evaluation of several days at one specific location has been used to estimate the weather-based influence on the harvestable energy. The paper also presented a methodology to analyze the possibility to supply embedded devices using energy harvesting systems. This methodology has been used to estimate the needed solar cell size for a continuous supply using energy harvesting at two different use cases. Future work will target the evaluation of further locations focusing also on industrial facilities and the long-term evaluation of energy harvesting devices.

Acknowledgement

This work has been supported in part by the COMET-K2 Center of the Linz Center of Mechatronics (LCM) funded by the Austrian federal government and the federal state of Upper Austria, and the InSecTT project. InSecTT (www.insectt.eu) has received funding from the ECSEL Joint Undertaking (JU) under grant agreement No 876038. The JU receives support from the European Union's Horizon 2020 research and innovation programme and Austria, Sweden, Spain, Italy, France, Portugal, Ireland, Finland, Slovenia, Poland, Netherlands, Turkey. The document reflects only the author's view and the Commission is not responsible for any use that may be made of the information it contains.

References

[1] M. Bal, Industrial applications of collaborative wireless sensor networks: A survey, 2014 IEEE 23rd International Symposium on Industrial Electronics (ISIE), June 2014, pp. 1463–1468; doi: 10.1109/ISIE.2014.6864830

[2] H.-P. Bernhard, A. Springer, A. Berger, and P. Priller, "Life cycle of wireless sensor nodes in industrial environments," in 13th IEEE Int. Workshop Factory Commun. Sys., Trondheim, Nor-way, May 2017; doi: 10.1109/WFCS.2017.7991943

[3] L. B. Hörmann, T. Buchegger, and C. Steger, Optimizing the Energy Supply of Autonomous Wireless Sensor Nodes, Microelectronic Systems Symposium (MESS 2014), 2014, pp. 1–6; doi: 10.1109/MESS.2014.7010257

[4] A. Janek, C. Trummer, C. Steger, R. Weiss, J. Preishuber-Pfluegl, and M. Pistauer, Simulation based Verification of Energy Storage Architectures for Higher Class Tags Supported by Energy Harvesting Devices, 10th Euromicro Conference on Digital System Design Architectures, Methods and Tools (DSD 2007), Lubeck, 2007, pp. 463-462.; doi: 10.1109/DSD.2007.4341510

[5] L.B. Hörmann, A. Berger, A. Pötsch, P. Priller, and A. Springer, "Estimation of the harvestable power on wireless sensor nodes," IEEE International Workshop on Measurements and Networking (MN 2015), 2015, 1-6; doi: 0.1109/IWMN.2015.7322964

[6] A. Kansal, D. Potter, and M. B. Srivastava, "Performance Aware Tasking for Environmentally Powered Sensor Networks", Proceedings of the joint international conference on Measurement and modeling of computer systems, ser. SIGMETRICS '04/Performance '04, 2004, pp. 223–234; doi: 10.1145/1005686

[7] T. Hölzl, "Drahtloses Messsystem für die Charakterisierung von Energy Harvesting Devices," master thesis, Institute for Communications Engineering and RF-Systems, Johannes Kepler University Linz, Austria, 2019.

[8] L. B. Hörmann, T. Hölzl, C. Kastl, P. Priller, and A. Springer, "Evaluation of Energy Harvesting Devices for Industrial Applications", Proceedings of the European Test and Telemetry Conference 2020 (ettc2020), 2020, pp. 31-37, doi: 10.5162/ettc2020/1.2

[9] Conrad Components SE, "Data Sheet – Solar cell 0.5V/400mA", Version 02/08, Item no. 19 12 81, https://asset.conrad.com/media10/add/160267/c1/-/gl/000191281DS01/datasheet-191281-conrad-components-yh-46x76-solar-panel.pdf, retrieved April 2022.

[10] Conrad Components SE, "Product Specification – Solar Cell Module Type YH-57X65", https://asset.conrad.com/media10/add/160267/c1/-/en/000191321DS01/datasheet-191321-conrad-components-yh-57x65-solar-panel.pdf, retrieved April 2022.

[11] IXYS KOREA LTD, "SM141K10LV – IXOLAR™ High Efficiency SolarMD", Rev. Sep. 2018, https://ixapps.ixys.com/DataSheet/SM141K10LV.pdf, retrieved April 2022.

[12] IXYS KOREA LTD, "SM141K09L – IXOLAR™ High Efficiency SolarMD", Rev. Sep. 2018, https://ixapps.ixys.com/DataSheet/SM141K09L.pdf, retrieved April 2022.

[13] SANYO Semiconductor Co., Ltd., "Amorphous Silicon Solar Cells / Amorphous Photosensors", Version 2007-11, https://media.digikey.com/pdf/Data%20Sheets/Sanyo%20Energy/Amorphous_Br.pdf, retrieved April 2022.

[14] L.B. Hörmann, T. Hölzl, C. Kastl, P. Priller, A. Springer, "Methode zur Evaluierung der Versorgungssicherheit von autarken Sensorknoten für industrielle Anwendungen", Automation 2020: Shaping Automation for our Future, VDI Verlag GmbH, 2020, doi: 10.51202/9783181023754

[15] Dependable Wireless Infrastructure, European Research project 2013-2017, http://www.dewiproject.eu

[16] Secure, connected and trustable things, European Research project 2017-2020, https://scottproject.eu/

[17] L. B. Hörmann, T. Hölzl, P. Priller, W. Neuwirth, H.-P. Bernhard, A. Springer, “Autarke Sensorknoten für industrielle IoT Anwendungen mit Multi-Sensor-Unterstützung,” in Innovation Messtechnik 2019, Linz, Austria, May 2019.

[18] S. Gezici, Z. Tian, G. Giannakis, H. Kobayashi, A. Molisch, H. Poor, and Z. Sahinoglu, “Localization via ultra-wideband radios: A look at positioning aspects for future sensor networks,” IEEE Signal Processing Magazine, vol. 22, pp. 70–84, 08 2005

[19] G. Avoine, M. Bingol, I. Boureanu, S. Capkun, G. Hancke, S. Kardas, C. Kim, C. Lauradoux, B. Martin, J. Munilla, et al., “Security of distance-bounding: A survey,” ACM Computing Surveys, 2017

[20] QUORVO, “DWM1001 Data Sheet”, https://www.decawave.com/dwm1001/datasheet/, retrieved April 2022